

PACS numbers: 52.50.Jm; 52.25.Tx; 42.55.Vc
DOI: 10.1070/QE2010v040n06ABEH014313

Charge exchange of multiply charged fluorine and lithium ions with Ne atoms

I.L. Beigman, E.A. Vishnyakov, M.S. Luginin, E.N. Ragozin, I.Yu. Tolstikhina

Abstract. **The charge exchange of multiply charged fluorine and lithium ions with Ne atoms in a gas jet was recorded from the line spectra in the 125–350 Å range, which arise from the radiative decay of the excited states of Li II–III and F III–VIII ions populated in the charge exchange. In the F III–VI ion spectra obtained from the plasma–gas interaction region we observed transitions from levels with an open (partly filled or completely open) 2s-shell, which may be populated in sequential events of single-electron charge exchange as well as in double- and many-electron charge exchange. Partial cross sections were calculated for the single-electron charge exchange of F VIII ions with Ne atoms. By way of Hartree–Fock energy level calculations it was possible to reveal resonances between the ground states of *k*-fold (*k* = 1–4) ionised donor atoms and the states of *k*-fold excited multiply charged fluorine ion resulting from the *k*-fold charge exchange of F VIII ions. These resonances may be responsible for the relatively large cross sections of double- and many-electron charge exchange.**

Keywords: *multiply charged ions, fluorine, single- and multielectron charge exchange, soft X-ray range, laser-plasma radiation source, imaging diffraction spectrometer, normal-incidence X-ray multilayer mirrors.*

1. Introduction

Our work is concerned with the experimental investigation of the charge exchange of fluorine and lithium ions with the atoms of a rare-gas jet (electron capture to the excited states of ions followed by their radiative relaxation)

$$X^{q+} + A \longrightarrow X^{*(q-k)+} + A^{k+},$$

where X^{q+} is an incident multiply charged ion; A is a neutral rare-gas atom (the donor atom); $X^{*(q-k)+}$ is the ion of multiplicity $q-k$ in an excited state [which is characterised by the principal (n) and orbital (l) quantum numbers in the case of single-electron charge exchange, $X_{nl}^{(q-1)+}$]; and A^{k+} is the resultant k-charged ion. Different values of $k = 1, 2, \ldots$ correspond to single-, double-, and multielectron charge exchange. In our experiment we recorded the line radiation arising from the radiative decay of the excited ion states populated in the charge exchange.

The interest in these processes is due to the fact that the resultant ion $X^{*(q-k)+}$ finds itself in an excited state and the charge-exchange cross section may amount to 10^{-15}–10^{-14} cm^2, which exceeds the cross sections of other elementary processes involving multiply charged ions. The quasi-resonance character of charge exchange makes it possible to selectively populate the levels of multiply charged ions and produce population inversion on their transitions in the soft X-ray (SXR) range [1–3]. Experimental research in this direction was earlier pursued and is presently underway [4, 5].

Experimental data [6] acquired in ion-beam experiments testify that double-electron charge-exchange cross sections for ions may be as high as the single-electron charge-exchange cross section, while three-electron charge-exchange cross sections may amount to 20%–30% of this value.

In the present work we recorded the charge exchange of multiply charged fluorine ions with Ne atoms from the line SXR radiation of the multiply charged ions arising from the radiative decay of excited states populated in the charge exchange. The fluorine ions were produced in the irradiation of a solid LiF target by the nanosecond pulses of a pulse-periodic laser. The LiF target was selected for the following reasons.

(i) The ions Li I–Li III possess only a few spectral lines in the 125–350 Å range under investigation. In the interpretation of charge-exchange spectra this permits virtually all lines to be unambiguously identified with the lines of fluorine atoms.

(ii) The strong transitions 1s–2p in Li III (135.0 Å) and $1s^2$–1s2p in Li II (199.28 Å) are good reference lines, which simplifies the procedure of determining the dispersion curve and facilitates the identification of spectral lines. The radiative transition wavelengths required in the identification of the spectra were borrowed from Refs [7].

Earlier in Refs [8, 9] an investigation was made of the charge exchange of carbon and boron ions with rare-gas atoms. Investigations with fluorine atoms are of fundamental importance in revealing the general tendencies for the charge-exchange cross sections of the ions of complex atoms (with a large atomic number). The objective of the present work was to investigate the charge exchange of multiply charged fluorine atoms with multielectron atoms (with Ne in the present case) employing the technique of imaging SXR spectroscopy. We had to abandon the idea of experimenting with O and N ions, because a convenient solid target is required in the generation of laser plasma.

I.L. Beigman, E.A. Vishnyakov, M.S. Luginin, E.N. Ragozin
P.N. Lebedev Physics Institute, Russian Academy of Sciences, Leninsky prosp. 53, 119991 Moscow, Russia; Moscow Institute of Physics and Technology (State University), Institutskii per., 9, 141700 Dolgoprudnyi, Moscow region, Russia;
e-mail: enragozin@sci.lebedev.ru;
I.Yu. Tolstikhina P.N. Lebedev Physics Institute, Russian Academy of Sciences, Leninsky prosp. 53, 119991 Moscow, Russia

Received 5 March 2010, revision received 26 April 2010
Kvantovaya Elektronika **40** (6) 545–550 (2010)
Translated by E.N. Ragozin

2. Experimental facility

Our experiments were performed in the IKAR vacuum chamber (∅ 0.9 × 3.8 m) equipped with an oil-free pump. The residual pressure in the chamber was no higher than 10^{-4} Torr. At the end of the vacuum chamber was a pulse-periodic laser utilising a neodymium-doped yttrium orthoaluminate crystal ($Nd:YAlO_3$, 0.5 J, 6 ns, 1.08 μm). The laser target was a ground disk of LiF rotated by an electric motor. The laser beam was focused to a spot with an effective area $S_{eff} \sim 10^{-5}$ cm^2 on the target with the use of a dense flint glass lens with a focal length $f = 75$ mm. The peak intensity of laser radiation at the centre of the focal spot was $\sim 10^{13}$ W cm^{-2}.

A pulsed Ne jet was produced by a pulsed electromagnetic valve with a supersonic nozzle whose opening was timed to a laser shot. The valve made use of a supersonic 10-mm-long conic nozzle with an outlet 1.0 mm in diameter and an outlet-to-input hole area ratio $S_{out}/S_{in} \approx 5.0$. The valve remained open for ~1.5 ms, the Ne stagnation pressure was made equal to 1.0–2.2 atm. The density distribution in the gas jet was earlier investigated from the absorption of $\lambda = 135$ Å backlighting radiation [10]. The density of Ne atoms on the jet axis was equal to $(1–2) \times 10^{18}$ cm^{-3}. The jet axis was parallel to the target plane and was spaced at ~1 cm from the target. The stream of multiply charged fluorine and lithium ions produced by focusing the nanosecond pulses on the solid LiF target was directed onto the supersonic Ne gas jet to give rise to charge exchange in the interaction with the jet (Fig. 1).

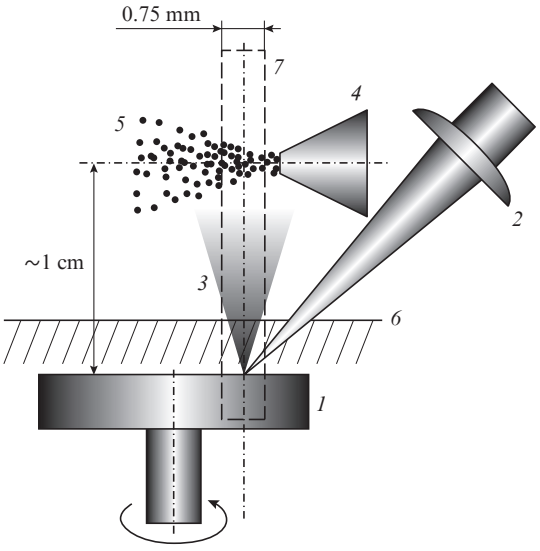

Figure 1. Mutual arrangement of the laser-plasma expansion cone (*3*) and the neon jet (*5*); (*1*) rotating target; (*2*) lens, which focuses laser radiation; (*4*) nozzle of the pulsed gas valve; (*6*) interrupter level; (*7*) field of view of the spectrograph.

Figure 2 shows the optical diagram of an imaging (stigmatic) diffraction SXR spectrograph [11], which possesses spatial resolution along one of the axes. The spectrograph is assembled on the 0.6 × 3.6 m optical table accommodated in the IKAR vacuum chamber and comprises an entrance slit, a broadband normal-incidence concave ($R = 1$ m) multilayer mirror (MM), a wide-aperture free-standing transmission diffraction grating (TG) (1000 lines mm^{-1}, 5 cm^2 area), and a film holder of radius 167 mm with UF-4 X-ray photographic

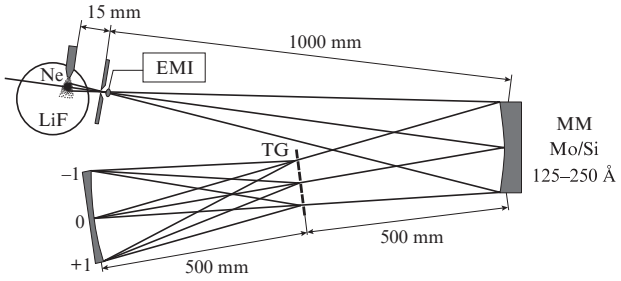

Figure 2. Schematic of the imaging diffraction spectrograph for the region $\lambda > 125$ Å.

film located at a distance $d = 500$ mm from the grating. (For small diffraction angles, the spectral focal curve is approximated by a circle of radius $d/3$.)

The wideband concave spherical MM serves as the focusing element of the spectrograph. This is a Mo/Si multilayer structure optimised for maximum uniform reflectivity in the 125–250 Å wavelength range [9, 11–13]; the L-edge of absorption in Si ($\lambda = 125$ Å) defines a sharp decrease of the mirror reflectivity in the domain $\lambda < 125$ Å and the short-wavelength bound of the operation range of the spectrograph. However, at wavelengths longer than 250 Å there are no prerequisites for a sharp fall in reflectivity, permitting the use of this spectrometer at longer wavelengths as well. In particular, in the irradiation of a magnesium target we observed the doublet $1s^22s\ ^2S_{1/2} - 1s^22p\ ^2P_{3/2,1/2}$ in MgX ion with wavelengths of 609.89 and 624.95 Å.

The entrance slit and the centre of the film holder are located on the Rowland circle associated with the concave MM. The distance between the detector centre and the entrance slit is equal to 210 mm, while the radius of curvature of the focusing MM is 1 m. The radiation reflection from the MM therefore takes place at small angles of incidence (~0.1 rad). As a result, the aberrations of the optical arrangement are small and the spectral images of the entrance slit on the sensitive detector surface are highly stigmatic.

The spectrograph's field of view (20 mm vertically) encompasses both the region of laser plasma emission near the solid target and the charge-exchange region, making it possible to record the spatial picture of plasma–gas interaction (Fig. 1). The distance of the axis of the plasma cone from the entrance slit is 15 mm, which gives a recorded zone width of 0.75 mm, taking into account the spectrograph's acceptance angle. The simultaneous recording of a large number of spectral lines in the charge-exchange region furnishes information about the distribution of charge-exchange products over ion multiplicities and energy levels with different n and l.

The spectra are recorded on UF-4 X-ray photographic film in several hundred laser shots. The plate scale for the spectra recorded is equal to 20 Å mm^{-1} and the spectral width of the entrance slit is 0.6 Å.

The total intensity of the line spectrum arising from the charge-exchange region is approximately an order of magnitude lower than that arising from hot plasma emission region at the target surface. However, it is expedient to deal with comparable exposure levels in different sections of the X-ray photographic film, which has a relatively narrow dynamic range. With this object in view, in the course of our experiments on exposing the film to some ten shots the domain of the field of view above ~3 mm from the target surface is shut

off by an electromagnetic interrupter (EMI) located near the entrance slit of the spectrograph (Fig. 2).

3. Experimental results and discussion

3.1. Spatial dependence of line intensities

One can see in Fig. 1 that the spectrograph's field of view includes both the surface of the LiF target and the region of the charge exchange of multiply charged fluorine and lithium ions in the gas jet. The spectrum of plasma emission near the target contains the spectral lines of the ions F III – F VIII and Li II – Li III (Fig. 3). The intensities of spectral lines decrease rapidly with distance from the target. However, in the plasma – gas interaction region the intensities of some of the lines start to increase again, which is testimony to the active population of excited states of plasma ions in the course of charge exchange. This kind of dependence of line intensities will be referred to as the 'charge-exchange-like' behaviour. In this case, the 'charge-exchange-like' behaviour of, for instance, the lines of the F III ion may correspond to the charge exchange of the ions F IV – F VII (depending on the charge-exchange multiplicity, $k = 1-4$), which results in the population of F III ion levels.

At the first stage of the investigation we made a series of 'probing' experiments for a non-sharp focusing of the laser beam. The spectra recorded in this case (Fig. 3a) contain charge-exchange lines of Li II, Li III and of the group of ions F III – F VI, testifying to the charge exchange of the Li III, Li IV, and F IV – F VII ions with Ne atoms. Characteristic of these spectra is the occurrence of relatively strong charge-exchange lines of the ions F III and F IV, which become substantially weaker with sharpening the laser pulse focusing on the target. This is best exemplified by the $2s^22p^3 - 2s^22p^2(^3P)3s$ transition (315.5 Å) in the ion F III (line C in Fig. 3a).

In the spectra recorded for a sharp focusing of laser radiation, the intensities of the F III and F IV ion lines are substantially weaker and there emerge strong charge-exchange lines of F V – F VIII ions. The strongest charge-exchange line in Fig. 3b arises from the $1s^22p - 1s^23d$ transition (127.7 Å) in the ion F VII (near the target this line is even stronger than the 135.0-Å line of the Li III ion).

It is customary to judge the sharpness of laser radiation focusing from near-target line intensity ratios between ions of different multiplicity. It can also be indirectly judged from the intensity ratio between the 135-Å (Li III, 1s – 2p) and 199.28-Å (Li II, $1s^2 - 1s2p$) lines in the charge-exchange region. In particular, a significant strengthening of the charge-exchange Li III line and, conversely, weakening of the Li II line is seen in passing from the spectrum in Fig. 3a to the spectrum in Fig. 3b, i.e. with sharpening the focusing. The 127.7-Å (F VII) to 315.5-Å (F III) line intensity ratio in the region of interaction with Ne is also a good indicator of the sharpness of laser radiation focusing on the target.

3.2. Characteristics of single-, double-, and multielectron charge exchange

In the interaction region we recorded three charge-exchange lines in each of the ions F VIII and F VII, 19 charge-exchange lines of F VI, 43 lines of F V, 54 lines of F IV, and 40 lines of F III. The strongest lines observed in the plasma – gas interaction region under a sharp laser radiation focusing on the target are collected in Table 1. The set of spectral lines excited in the plasma – gas interaction region does not coincide with the set of lines emitted in the hot plasma region at the target;

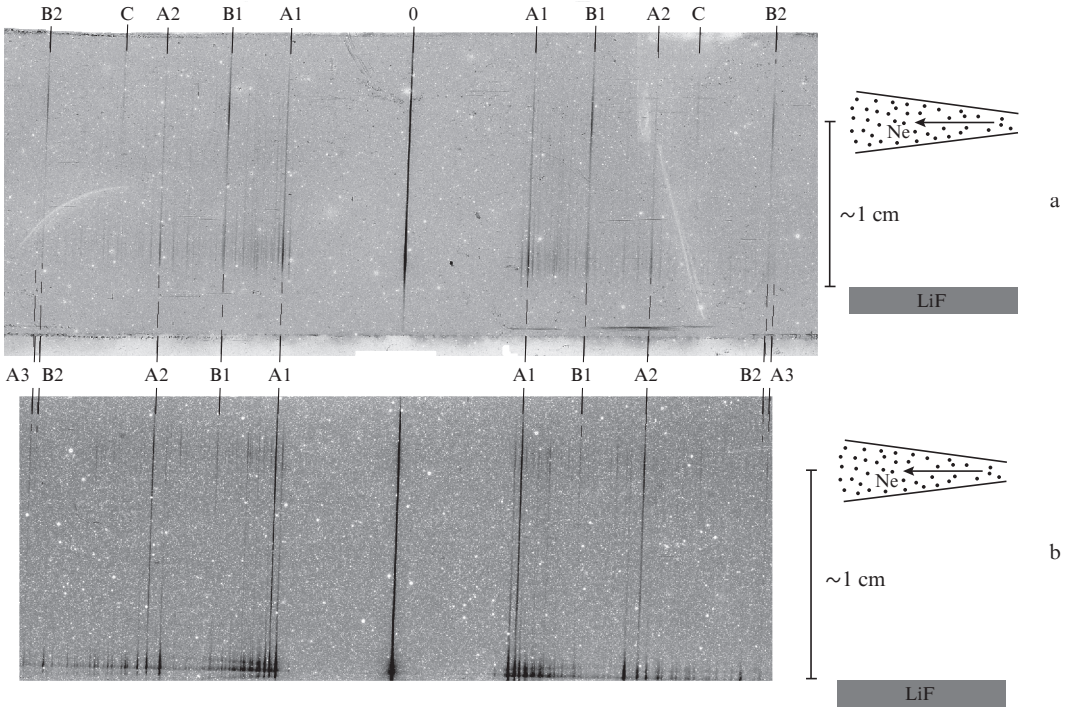

Figure 3. Charge-exchange spectra obtained for non-sharp (a) and sharp (b) radiation focusing on the target. Lines A1 – 3 correspond to the 135.0-Å line of Li III in different diffraction orders, lines B1,2 correspond to the 199.28-Å line of Li II, and line C to the 315.5-Å line of F III.

Table 1. Strongest lines in the charge-exchange spatial region of the spectrogram.

λ (Å)	Ion $X^{*(q-k)+}$	Recorded radiative transition	Charge-exchange multiplicity	Probable acceptor
127.7–127.8	F VII	$1s^22p(^2P^0)-1s^23d(^2D)$	1	F VIII
129.5	F VI	$2p^2-2p4s$	2	F VIII
132.5	F V	$2s2p^2(^4P)-2s2p(^3P^0)4d(^4D^0)$	2	F VII
135.0	Li III	1s–2p	1	Li IV
136.9	F V	$2s2p^2(^4P)-2p^2(^3P)3p(^4D^0)$	3	F VIII
138.2	F V	$2s2p^2-2s2p(^3P^0)4s$	2	F VII
139.8–139.9	F VI	$2s2p(^3P^0)-2s3d(^3D)$	1	F VII
145.2	F V	$2s2p^2(^2D)-2s2p(^3P^0)4d(^2D^0)$	2	F VII
147.9–148.1	F V	$2s2p^2(g^2P^0)-2s2p(^3P^0)3p(^2D)$	2	F VII
153.7–153.9	F VI	$2s2p(^3P^0)-2s3s(^3S)$	1	F VII
156.2	F VI	$2s2p(^1P^0)-2s3d(^1D)$	1	F VII
158.5	F V	$2s2p^2(^2D)-2s2p(^1P^0)3d(^2F^0)$	2	F VII
161.2–161.5	F VI	$2p^2(^3P)-2p(^2P^0)3s(^3P^0)$	2	F VIII
163.5–163.6	F V	$2s2p^2(^4P)-2s2p(^3P^0)3d(^4D^0)$	2	F VII
166.0–166.2	F V	$2s^22p-2s^23d$	1	F VI
178.4–178.6	F V	$2s2p^2(^2D)-2s2p(^3P^0)3d(^2F^0)$	2	F VII
183.0	F V	$2s2p^2(^2D)-2s2p(^3P^0)3d(^2D^0)$	2	F VII
186.7–187.0	F V	$2s2p^2(^4P)-2s2p(^3P^0)3s(^4P^0)$	2	F VII
190.6–190.8	F V	$2s^22p-2s^23s$	1	F VI
191.9–192.0	F V	$2s2p^2(^2S)-2s2p(^3P^0)3d(^2P^0)$	2	F VII
199.28	Li II	$1s^2-1s2p$	1	Li III
208.3	F IV	$2s^22p^2(^1D)-2s^22p(^2P^0)3d(^1F^0)$	1	F V
208.5	F IV	$2s2p^3(^3P^0)-2s2p^2(^2D)3d(^3S)$	3	F VII
240.1	F IV	$2s^22p^2(g^3P)-2s^22p(^2P^0)3s(^3P^0)$	1	F V
251.0	F IV	$2s^22p^2(^1D)-2s^22p(^2P^0)3s(^1P^0)$	1	F V

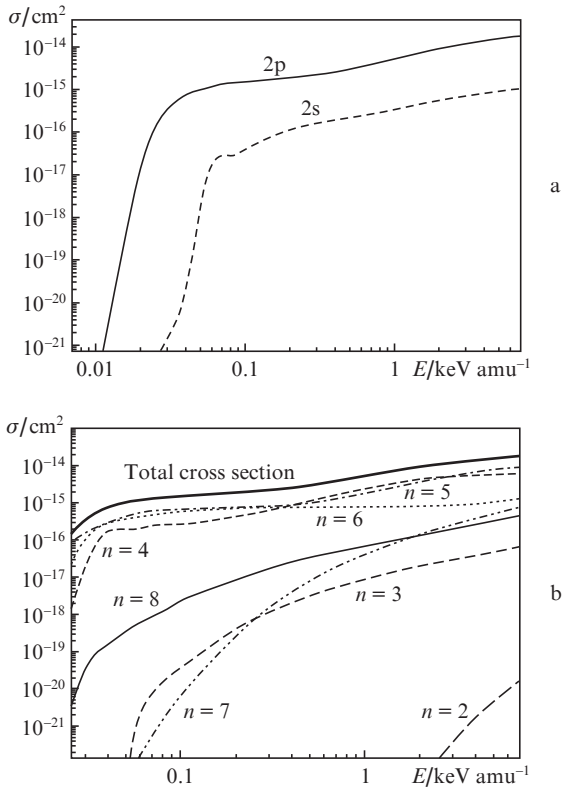

Figure 4. Cross section for the single-electron charge exchange of F VIII ions with neon atoms as a function of collision energy: contribution of s and p electrons of Ne (a) as well as partial charge-exchange cross sections for levels with $n = 2-8$ of the F VII ion and total charge-exchange cross section (b).

also different are their ratios. This applies both to the ratios between line intensities of a specific ion and to the ratios between the intensities of lines of different ions.

Attention is drawn to the fact that about 15 lines in the charge-exchange region belonging to the ions F IV–F VI arise from transitions from levels with an unfilled (partly filled or completely vacant) 2s shell. These are the $2p^2-2p4s$ (F VI, $\lambda = 129.5$ Å), $2s2p^2-2p^23p$ (F V, 136.9 Å), $2s2p^2-2s2p4s$ (F V, 138.2 Å), and $2s2p^3-2s2p^23d$ (F IV, 208.5 Å) transitions. The states of this kind are not populated in collisions with electrons in a cold tenuous plasma. In the plasma–gas interaction region these levels may be populated in two ways. First, in the sequential single-electron charge exchange when the frequency $N_{Ne}\sigma_{CE}v$ of single-electron charge-exchange events exceeds the characteristic radiative transition probability $A(2p \rightarrow 2s)$. Here, N_{Ne} is the density of neon atoms, σ_{CE} is charge-exchange cross section, and v is the ion velocity. Second, in the double-, triple-, and multielectron charge exchange ($k = 2, 3, ...$) into states with k excited electrons. The charge-exchange multiplicity k may be judged from the number of electrons in the excited states of the resultant multiply charged ions $X^{*(q-k)+}$ in the charge-exchange region (strictly speaking, the multiplicity may be greater than the number of excited electrons in the initial level of the transition if a part of the electrons has had time to relax or escape to the continuous spectrum as a result of an Auger transition).

Sequential single-electron charge exchange. In our experiment, in the case of transit through the paraxial region of the gas jet the free path of fluorine ions relative to single-electron charge exchange was much shorter than the jet diameter, and the frequency of single-electron charge exchange events in this region was $\sim 10^{10}$ s^{-1}, which is much higher than the characteristic probability of allowed radiative transitions $A(2p \rightarrow 2s) \sim 10^8-10^9$ s^{-1}. This makes possible the population of levels with an unfilled 2s-shell in the sequential charge exchange of fluorine atoms in collisions with different donor atoms.

The plasma generated in the central part of the focal spot is dominated by He-like F VIII ions. Calculations of the partial charge-exchange cross sections show that the total cross section for single-electron F VIII ion charge-exchange with Ne atoms is almost entirely due to the p-shell electrons of Ne and in the collision energy range of interest [0.05–0.8 keV nucleon^{-1}, which corresponds to the characteristic ion velocities of $(1-4)\times 10^7$ cm s^{-1}] is equal to $\sim 10^{-15}$ cm^2 (Fig. 4). In this case, the main contribution to the total cross section is made by the partial charge-exchange cross sections for levels with $n = 5$ and 6, which have energies closest to the ionisation energy of Ne atoms, as well as for level with $n = 4$ (for collision energies of ~ 0.3 keV nucleon^{-1} and above). The partial charge-exchange cross sections were calculated by the ARSENY code [14] elaborated by E.A. Solov'ev on the basis of the effect of hidden crossing of quasimolecular levels.* This effect was first discovered in Ref. [15].

* The experimental data on charge-exchange cross sections available from the literature were acquired in ion-beam experiments and pertain to total charge-exchange cross sections. Greenwood et al. [6] give the cross section for the charge exchange of carbon nuclei with He for a collision energy of 3.23 keV nucleon^{-1}: $\sigma(C^{6+} + He) = (1.5\pm 0.2)\times 10^{-15}$ cm^2. In an earlier work by Janev et al. [16] the cross section for this reaction was measured at $(0.9\pm 0.4)\times 10^{-15}$ cm^2 for a collision energy of 2 keV nucleon^{-1}. Our calculations at these energies yield a value of 1.1×10^{-15} cm^2. Comparing these data allows a conclusion about good agreement between calculations and experiment.

Multielectron charge exchange. Qualitative considerations and an analogy with single-electron charge exchange suggest that the probability of double- and multielectron charge exchange may be significant in resonance conditions. The case in point is the coincidence of the energy of k-electron capture to the excited state $X^{*(q-k)+}$ with the energy required to detach k electrons from a neutral atom (the energy of k-fold ionisation). Hartree–Fock calculations of the energy levels of fluorine ions revealed the existence of resonances between certain terms of the ground electron configuration of a k-fold ionised donor atom and the k-fold excited multiply charged ion resulting from charge exchange. In the majority of cases, by the ground electron configuration of the resultant Ne ion is meant the $2s^2 2p^{6-k}$ configuration. The $2s2p^{6-(k-1)}$ and $2p^{6-(k-2)}$ configurations should also be borne in mind, but the analogy with single-electron charge exchange suggests that the contribution of s electrons to the cross section may turn out to be appreciably smaller than the contribution of p electrons (Fig. 4a).

The potentials of k-fold ionisation of Ne (so far we are dealing with the lowest term of the ground electron configuration) are equal to 21.6, 62.5, 126.0, and 223 eV for $k = 1-4$, respectively. When the ion $X^{*(q-k)+}$ has an excited state such that the binding energy of k electrons is only slightly different from the corresponding ionisation potential of Ne (to within 1–2 eV), the k-fold charge exchange of the ion X^{q+} may take place in a resonance way. As this takes place the insignificant defect in binding energy is compensated by the corresponding change in kinetic energy of the interacting particles. Our calculations by the Hartree–Fock method show that the ions $X^{*(q-k)+}$ for $k = 2$ and 3 possess groups of states (which differ by the values of their orbital quantum numbers) which are at resonance with the terms of the ground state of k-fold ionised Ne to within ±2 eV. By way of example Fig. 5 shows the resonances with the lowest terms of the ground electron configuration of neon ions produced in the interaction F VIII ($1s^2$) + Ne. In particular, the ^3P term of doubly ionised neon Ne III (62.5 eV) is at resonance with the $1s^2 4l'5l''$ states of the ion F VI, and the ^4S term of triply ionised neon Ne IV (126.0 eV) is at resonance with the $1s^2 3l'4l''5l'''$ of the ion F V. The states (k-fold excited) $X^{*(q-k)+}$ may subsequently populate – by way of (cascade) radiative decay – the states which give rise to SXR transitions recorded in our experiment.

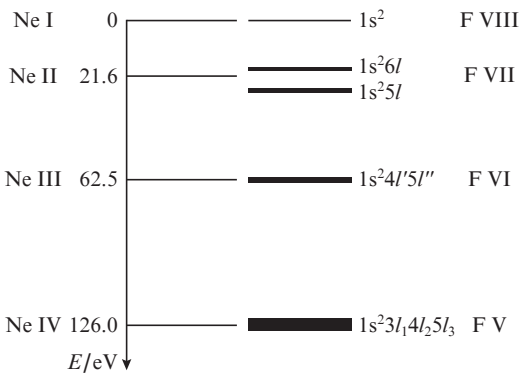

Figure 5. Energy diagram of the single-, double-, triple-electron charge exchange F VIII ($1s^2$) + Ne. Shown are only the resonances with the lowest terms of the ground electron configuration of the ions Ne III and Ne IV.

In the foregoing we were dealing only with resonances which take place in the charge exchange involving the production of Ne ions in the lowest term of the ground electron configuration. However, all terms should be taken into account in the search for resonances. The $2s^2 2p^5$ electron configuration of the ion Ne II is represented by the term $^2P_{3/2,1/2}$ with the separation of its components of only 0.097 eV. Meanwhile, the ground electron configuration $2s^2 2p^4$ of the ion Ne III is represented by three terms: $^3P_{2,1,0}$, $^1D_2$, and $^1S_0$. If the energy of the $^3P_2$ level is assumed to be zero, the energies of the terms $^1D_2$ and $^1S_0$ will be equal to 3.2 and 6.9 eV [the spacings between the multiplet components are small (~ 0.1 eV)]. The ground electron configuration $2s^2 2p^3$ of the ion Ne IV is represented by the terms $^4S_{3/2}$, $^2D_{5/2,3/2}$, and $^2P_{1/2,3/2}$, the two last-named terms lie 5.1 and 7.7 eV above the $^4S_{3/2}$ term. The ground electron configuration $2s^2 2p^2$ of the ion Ne V is represented by the terms $^3P_{0,1,2}$, $^1D_2$, and $^1S_0$. If the energy of the $^3P_0$ level is taken to be zero, the energies of the terms $^1D_2$ and $^1S_0$ will be equal to 3.8 and 7.9 eV.

Therefore, the inclusion of all terms of the ground electron configuration will result in the emergence of additional horizontal lines on the Ne side in Fig. 5 but will not change the picture qualitatively, since their energies differ by no more than 8 eV from the energies of the lines already indicated. If we take into account the terms of the $2s2p^{6-(k-1)}$ and $2p^{6-(k-2)}$ configurations, which lie above the terms of the $2s^2 2p^{6-k}$ configuration, additional resonance overlappings may emerge in the energy diagram. In view of the resonance width of ~ 2 eV, the terms of these configurations make up energy bands between the levels indicated in Fig. 5. For the Ne III ion, in particular, the terms of the $2s2p^5$ configuration are located in the 25–36 eV energy band, and the term ^1S of the $2p^6$ configuration has an energy of 59.4 eV (for an ionisation potential of 63.4 eV). In the Ne IV ion, the terms of the $2s2p^4$ configuration lie in the 31.5–39.8 eV band, and the terms of the $2p^5$ configuration lie in the vicinity of 60 eV (for an ionization potential of 97.1 eV). This signifies that in the domain of possible resonances in Fig. 5 there will emerge additional bands in the 60–195 eV range, which supposedly make a somewhat smaller contribution to the charge-exchange cross section than the terms of the $2s^2 2p^{6-k}$ configuration.

We believe that both mechanisms (sequential single-electron charge exchange and the multielectron one) may be responsible to an extent for populating the $X^{*(q-k)+}$ ion levels, including the levels with an unfilled 2s-shell. It is anticipated that the relative contributions of these mechanisms may be separated in experiments with a lower density of the gas jet. On lowering the density by approximately two orders of magnitude, free path of fluorine ions relative to charge exchange will exceed the characteristic jet diameter (1 mm), making sequential single-electron charge exchange unlikely.

4. Conclusions

This work is concerned with the study of the interaction between multiply charged F and Li ions and Ne atoms in a pulsed gas jet. Partial cross sections were calculated for the single-electron charge exchange of F VIII ions with Ne atoms. The charge exchange of multiply charged fluorine and lithium ions was recorded from the line spectra in the 125–350 Å range, which emerged in the radiative decay of the excited states of the ions Li II–III and F III–VIII populated in the charge exchange. The spectra were recorded employing an SXR diffraction spectrometer with spatial resolution. In the

ions F III–F VI we recorded transitions originating from the states with an unfilled (partly or completely) 2s shell. Two mechanisms responsible for populating them were proposed:

– sequential single-electron charge exchange with different neon atoms;

– double- and multielectron charge exchange of F ions with Ne atoms.

The energy levels of k-fold ($k = 1–4$) excited multiply charged ion were calculated using the Hartree–Fock method. Resonances were discovered between the k-fold-ionisation potentials of Ne atoms and the energy of capture of k electrons to the excited states of certain fluorine ions. This may qualitatively account for the relatively large multielectron charge-exchange cross sections. In passing to the interaction of 'complex' multiply charged ions with multielectron atoms, double- and multielectron charge exchange comes to play a significant role in the population of excited states of the ions and formation of their spectra.

Acknowledgements. The authors express their appreciation to E.A. Solov'ev for placing the ARSENY code at our disposal. This work was partly supported by the Russian Foundation for Basic Research (Grant No. 07-02-00316).

References

1. Presnyakov L.P., Shevel'ko V.P. *Pis'ma Zh. Eksp. Teor. Fiz*., **13**, 286 (1971).
2. Vinogradov A.V., Sobel'man I.I. *Zh. Eksp. Teor. Fiz.*, **63**, 2113 (1972).
3. Presnyakov L.P., Ulantsev A.D. *Kvantovaya Electron*., **1**, 2377 (1974) [*Sov. J. Quantum Electron.*, **4**, 1320 (1974)].
4. Dixon R.H., Seely J.F., Elton R.C. *Phys. Rev. Lett*., **40** (2), 122 (1977).
5. Kawachi T., Kado M., Tanaka M., Hasegawa N., Nagashima A., Kato Y. *J. Phys. IV*, **11**, Pr.2–255 (2001).
6. Greenwood J.B., Williams I.D., Smith S.J., Chutjian A. *Astrophys. J*., **533**, L175 (2000); *Phys. Rev. A*, **63**, 062707 (2001).
7. Kelly R.L. *J. Phys. Chem. Ref. Data*, **16**, Suppl. 1 (1987); http://physics.nist.gov/PhysRefData/ASD/levels_form.html.
8. Beigman I.L., Levashov V.E., Mednikov K.N., Pirozhkov A.S., Ragozin E.N., Tolstikhina I.Yu. *Kvantovaya Electron*., **37** (11), 1060 (2007) [*Quantum Electron.*, **37** (11), 1060 (2007)].
9. Ragozin E.N., Mednikov K.N., Pertsov A.A., Pirozhkov A.S., Reva A.A., Shestov S.V., Ul'yanov A.S., Vishnyakov E.A. *Proc. SPIE Int. Soc. Opt. Eng.*, **7360**, 73600N (2009).
10. Boldarev A.S., Gasilov V.A., Levashov V.E., Mednikov K.N., Pirozhkov A.S., Pirozhkova M.S., Ragozin E.N. *Kvantovaya Electron*., **34** (7), 679 (2004) [*Quantum Electron.*, **34** (7), 679 (2004)].
11. Kondratenko V.V., Levashov V.E., Pershin Yu.P., Pirozhkov A.S., Ragozin E.N. *Kratk. Soobshch. Fiz.*, **7**, 32 (2001).
12. Ragozin E.N., Kondratenko V.V., Levashov V.E., Pershin Yu.P., Pirozhkov A.S. *Proc. SPIE Int. Soc. Opt. Eng*., **4782**, 176 (2002).
13. Vishnyakov E.A., Mednikov K.N., Pertsov A.A., Ragozin E.N., Reva A.A., Ul'yanov A.S., Shestov S.V. *Kvantovaya Electron.*, **39** (5), 474 (2009) [*Quantum Electron.*, **39** (5), 474 (2009)].
14. Solov'ev E.A. *Proc. XIX ICPEAC*. Ed. by Dube L.J. et al. (New York: AIP Press, 1995) p. 471.
15. Solov'ev E.A. *Usp. Fiz. Nauk*, **157** (3), 437 (1989) [*Sov. Phys. Usp*., **32** (3), 228 (1989)].
16. Janev R.K., Phaneuf R.A., Hunter H.T. *At. Data Nucl. Data Tables*, **40**, 249 (1988).